

# Acoustic nonlinear amplitude versus angle inversion and data-driven depth imaging in stratified media derived from inverse scattering approximations

Lasse Amundsen<sup>1,2</sup>, Arne Reitan<sup>3</sup>, Børge Arntsen<sup>1</sup> and Bjørn Ursin<sup>2</sup>

<sup>1</sup> Statoil Research Centre, Posttuttak, N-7005 Trondheim, Norway

<sup>2</sup> Department of Petroleum Engineering and Applied Geophysics, The Norwegian University of Science and Technology, N-7491 Trondheim, Norway

<sup>3</sup> Skomakerveien 14, N-4839 Arendal, Norway

E-mail: [lam@statoil.com](mailto:lam@statoil.com)

Received 20 April 2006, in final form 16 August 2006

Published 27 September 2006

Online at [stacks.iop.org/IP/22/1921](http://stacks.iop.org/IP/22/1921)

## Abstract

This paper presents a new theory for nonlinear direct amplitude versus angle (AVA) inversion and data-driven depth imaging for a depth-variable acoustic medium. The method which is derived by direct inversion of the forward model of acoustic single scattering requires no information of the velocity and density potentials (subsurface properties), except for the velocity and density of the uppermost layer which is the reference medium where the source and receiver are situated at a finite distance above the scattering medium. The vertically varying velocity and density of the scattering medium are estimated in a data-driven manner solely from the angle- and depth-dependent Born potential profile. The inversion method is obtained in three main steps. In step one, the Born potential profile is computed by constant-velocity imaging (migration) of the single scattering data in the time intercept-slowness domain. Generally, interfaces in the Born potential are severely mislocated in depth compared to the true potential. In step two, ‘squeezed’ depth-dependent velocity and density potentials are estimated by nonlinear direct AVA inversion of the Born potential after residual-moveout correction. Step three estimates the actual depth-dependent velocity and density potentials by stretching the squeezed potentials so that their interfaces are moved towards the correct depth. In the nomenclature of seismic processing, the three steps can be described by the sequence constant-velocity (partial) migration–inversion–residual migration. In contrast to conventional, velocity-dependent depth migration, which requires an accurate estimate of the velocities of the actual medium to obtain the proper image, the depth imaging in step three requires the squeezed actual velocity potential with interfaces matching those of the zero-angle Born potential depth profile. This is exactly the velocity potential that is found in step two.

## 1. Introduction

A key and the most serious challenge in seismic imaging and inversion today is the inability to find an adequate image beneath complex heterogeneous media. This is a universally recognized issue in the geophysical exploration community. However, there are approaches and research efforts underway today that implicitly or explicitly recognize that state of affairs and offer a spectrum of different responses to that challenge. We would like to begin by providing a brief perspective of those methods and responses and then we will place the contribution of this paper within that overall context.

The response has been in two basic different approaches and categories: (i) to seek to improve the satisfaction of conditions and prerequisites for current seismic imaging and (ii) to provide fundamentally new seismic imaging concepts that totally avoid the limiting assumptions behind current imaging techniques.

The methods in category (i) currently most often correspond to indirect inversion. Indirect inversion methods seek to satisfy a property associated with a desired solution, and in that way indirectly produce a solution. Often a search engine is involved seeking to minimize an objective function, which can be a mismatch between synthetic or actual data, or a criteria for searching offset trajectories, with different degrees of freedom, seeking, e.g., either an optimal stack or a residual moveout for a horizontal common image gather. The key references are Ursin (1982), Hubral (1999), Gelchinsky *et al* (1999), Landa *et al* (1999) and Berkhout and Verschuur (2001). An advantage of these indirect methods is their ease of understanding of searching around until something fits, bringing with it broader audience acceptance, but at the cost perhaps of moving away from physics and towards belief in and attraction to optimization search engines.

The methods in category (ii) frequently fall into the area of direct inversion, although not exclusively. Direct methods provide algorithms that explicitly solve for and produce the stated processing objective. In direct methods, there were really three historic approaches. First, linear methods that assumed that an adequate velocity could be determined for imaging and furthermore that the changes in earth material properties across an interface could be well approximated by a linear form. Linear methods contain all current migration methods (e.g., finite difference, beam, FK, plane wave or Kirchhoff), and linear inverse methods, and inversion methods based on e.g. Bortfeld, Aki and Richards, linear approximate relationships. Among those who pioneered these methods are Claerbout (1971), Secret (1975), Schneider (1978), Stolt (1978), Gazdag (1978), French (1978), Cohen and Bleistein (1977), Berkhout (1982), Clayton and Stolt (1981) and Stolt and Weglein (1985). A review of parameter inversion and angle migration in anisotropic elastic media is given in Ursin (2004). Second, iterate linear inverse, a nonlinear method where the solved for first linear estimated perturbation in medium properties would be added to the original reference or background to update the background towards the actual medium properties. Iterative linear inverse had a flurry of activity in the 1980s where the key references are Keys and Weglein (1983), Lailly (1984), Ikelle (1986), Tarantola (1987), Cao (1989) and Beydoun and Mendes (1989). Third, the inverse scattering series and isolated task-separated subseries. For an introduction to the inverse scattering series in the seismic field, the reader is referred to the series of papers by Weglein *et al* (2000, 2002, 2003), Innanen (2003), Innanen and Weglein (2003), Shaw *et al* (2004), Shaw and Weglein (2004), Shaw (2005), Zhang and Weglein (2005), Liu *et al* (2005) and Ramirez and Weglein (2005). The inverse scattering series was originally, and remains today, the only comprehensive direct methodology that can accomplish all of the tasks associated with seismic processing objectives directly in terms of reflection data, and a simple (e.g., homogeneous water speed) reference propagation that is never updated or moved towards the actual. All

inverse steps are essentially migration in water speed, yet its potential is to directly address the most complex challenges. This potential has been realized for free surface and internal multiple removal under difficult geologic conditions, and this promise is being pursued for imaging and inverting primaries, with very promising multi-dimensional synthetic tests and algorithm development.

Recently, Amundsen *et al* (2005a, 2005b) have published papers using 1D inverse scattering formalism and seeking non-series approximate solutions to imaging objectives associated with primaries. Recognizing that the integrals that appear in the closed-form leading-order 1D imaging subseries derived by Shaw *et al* (2004) and Shaw (2005), and discussed in Innanen (2003), exhibited an approximate eikonal form, it triggered that there could be an analogous forward approximate scattering model based on the eikonal, or its generalization, the WKBJ approximation. We refer to Morse and Feshbach (1953), Schiff (1955 and later editions), Glauber (1959), Joachain (1975) and Bransden and Joachain (1989) for a description of the physical basis and applications of the eikonal and WKBJ methods. Based on the experience from the research reported on the closed-form leading-order 1D imaging subseries, Amundsen and coworkers launched research into establishing a new derivation of those imaging results by considering the inversion of the WKBJ scattered field and were able to recast and reproduce those earlier available 1D results without resorting to a series. In particular, they showed that for a piecewise-constant 1D velocity-varying medium, the inverse WKBJ scattering solution could be formed by the three steps of constant-velocity migration, inversion and residual migration. After constant-velocity migration, layer velocities are erroneous and layer interfaces are wrongly positioned. The direct, non-iterative inversion step gives an estimate of the true layer velocities, but does not adjust the depth of the layer interfaces. From these velocity estimates, the residual migration moves the layer interfaces to their approximately true depths. Observe that in contrast to conventional depth migration, which requires the correct depth velocity model to obtain the correct depth image, the residual migration requires correct layer velocities but interfaces at the wrong depths, that is, the depths provided by the constant-velocity migration.

The current paper provides further insights into the amplitude versus angle (AVA) application of the WKBJ forward model and relates these to earlier inverse series efforts and the results of Zhang and Weglein (2005), again here without a series, and provides the same conceptual benefit, new insight and guidance within its context, to the overall campaign pursued by the inverse scattering series. Insights and different perspectives and derivations on previous results are important factors contributing to further advances in the inverse scattering imaging and inversion series. However, with further and more complete 3D imaging efforts, we anticipate being able to capture imaging capability without a closed form, and therefore without a single-step non-series approximate inverse.

More specifically, the main objective of the present paper is to extend the work in Amundsen *et al* (2005b) from a 1D normal-incidence scattering model to a 3D scattering model for a depth-variable velocity and density acoustic medium. The current paper, which has a different starting point from the earlier imaging papers, is organized as follows. First, we derive a simple physical model for single scattering of acoustic waves from a stratified medium. The incident downgoing wave is described by the zero-order WKBJ approximation. The scattered wave is described by the first-order WKBJ approximation which takes into account the coupling of the incident wave with the scattered wave (Bremmer 1951; Ursin 1984, 1987). Second, the forward model is used as the mathematical framework for relating the angle-dependent Born potential to the single scattering response of a stratified acoustic medium. Using the known constant velocity and density reference medium, the angle-dependent Born potential is simply obtained by trace integration of the scattered data transformed to the

time intercept-slowness domain, by which the primary reflection events are placed at depths computed linearly only using the constant reference velocity and the traveltimes of primaries. From the angle-dependent residual moveout-corrected Born potential, amplitude versus angle inversion gives an estimate within the layer boundaries of the zero-angle Born potential depth profile of what the depth-dependent velocity and density potentials would be. Since the layer boundaries are severely mislocated in the zero-angle Born potential depth profile, the AVA analysis produces estimates of the amplitude of the actual velocity and density potentials but at wrong depths. We denote the mislocated velocity and density potentials by ‘squeezed’ potentials, as they appear like the actual velocity and density potentials when the depth axis is squeezed. From the information in the squeezed velocity potential, we show in the WKBJ approximation that the reflector positions in both the squeezed velocity and squeezed density potentials can be moved with high precision towards their correct spatial location without introducing any information about the subsurface. Finally, a simple example is constructed to show how the procedures introduced in this paper can be applied to obtain the velocity and density potentials and the corresponding velocities and densities for the stratified acoustic medium.

Note that the inverse scattering problem to be analysed in the present paper is limited to that of processing acoustic single scattering events, or equivalently, primaries. As any real acoustic data from a layered medium will contain both primaries and multiples, real data have to go through a preprocessing step to remove all types of multiples before applying the proposed inversion/depth imaging steps to be presented. The preprocessing is in agreement with the standard practice to seek to attenuate all multiples from acoustic (seismic) data before using primaries for imaging changes in the medium’s properties (see, e.g., Weglein *et al* (1997) and Ikelle and Amundsen (2005)). The historical evolution and development of seismic processing and inversion explain the motivation for addressing the inverse acoustic scattering problem as that of inverting primaries.

## 2. The forward scattering model

In this section, we present the forward model of acoustic single scattering. For a stratified medium, it is a standard procedure to transform the physical field variables by applying a Fourier transform with respect to time and horizontal spatial coordinates. This transforms the acoustic equations into a system of first-order differential equations.

Let  $t$  denote time and  $(x, y, z)$  the Cartesian coordinates. The depth axis is positive downwards. The acoustic medium, where the wave velocity and density are functions of depth,  $c = c(z)$ ,  $\rho = \rho(z)$ , respectively, is embedded in a homogeneous reference medium with wave velocity  $c_0$  and density  $\rho_0$ . The system of equations governing the wave motion consists of the pressure–particle velocity relation (the time derivative of Hooke’s law) and the equation of motion:

$$\nabla \cdot \mathbf{v}(x, y, z, t) + \frac{1}{M(z)} \frac{\partial p(x, y, z, t)}{\partial t} = \frac{\partial i_v(x, y, z, t)}{\partial t}, \quad (1)$$

$$\nabla p(x, y, z, t) + \rho(z) \frac{\partial \mathbf{v}(x, y, z, t)}{\partial t} = 0, \quad (2)$$

where  $p$  is the pressure,  $\mathbf{v}$  is the particle velocity vector,  $M = \rho c^2$  is the bulk modulus and  $i_v$  is a source distribution which represents a volume density of volume injection (for example, an airgun source). A monopole point source at  $x = y = z = 0$  is represented by

$$\rho \frac{\partial^2 i_v(x, y, z, t)}{\partial t^2} = \delta(x)\delta(y)\delta(z)a(t),$$

where  $a(t)$  is the source signature and  $\delta(x)\delta(y)\delta(z)$  represents a 3D spatial Dirac delta function. The boundary conditions state continuity of pressure and vertical component of particle velocity at the interfaces. In addition, we impose the radiation conditions that the only downgoing wave in the source layer is that radiated by the source and that there are no upgoing waves in the lower halfspace.

We introduce the Fourier transform with respect to time and horizontal spatial coordinates

$$G(k_x, k_y, \omega) = \int_{-\infty}^{\infty} \int_{-\infty}^{\infty} \int_{-\infty}^{\infty} dx dy dt \exp[-i(k_x x + k_y y - \omega t)] g(x, y, t), \quad (3)$$

with inverse

$$g(x, y, t) = \frac{1}{(2\pi)^3} \int_{-\infty}^{\infty} \int_{-\infty}^{\infty} \int_{-\infty}^{\infty} dk_x dk_y d\omega \exp[i(k_x x + k_y y - \omega t)] G(k_x, k_y, \omega). \quad (4)$$

Here,  $\omega$  denotes circular frequency and  $(k_x, k_y)$  are horizontal wavenumbers conjugate to  $(x, y)$ . Furthermore, we introduce the radial wavenumber  $k_r^2 = k_x^2 + k_y^2$ , the horizontal slownesses  $p_x = k_x/\omega$  and  $p_y = k_y/\omega$ , the radial slowness (ray parameter)  $p^2 = p_x^2 + p_y^2$  and the vertical wavenumber  $K_z(z) = \sqrt{\omega^2 c^{-2}(z) - k_r^2}$ . In the reference medium, the wavenumber is denoted by  $k = \omega/c_0$  and the vertical wavenumber is denoted by  $k_z = \sqrt{\omega^2 c_0^{-2} - k_r^2}$ . We also introduce the vertical slowness in the reference medium  $q = k_z/\omega$ . For notational convenience, we define

$$\kappa = k k_z^{-1}.$$

In the reference medium, a plane wave is described by its frequency  $\omega$  and direction of travel

$$\theta = \arcsin(c_0 p). \quad (5)$$

The angle  $\theta$  is measured as the ray's angle from the  $z$ -axis to the ray. Then,  $\kappa^{-1} = \cos \theta = \sqrt{1 - (c_0 p)^2} = c_0 q$ .

The Fourier transform of equations (1) and (2) leads to the first-order wave equation for pressure  $P$  and vertical component of particle velocity  $V_z$  (Ursin 1983, Claerbout 1985)

$$\frac{d}{dz} \mathbf{B}(z) = \mathbf{A}(z) \mathbf{B}(z) + \mathbf{\Sigma}(z), \quad (6)$$

with field vector

$$\mathbf{B}(z) = \begin{bmatrix} P(z) \\ V_z(z) \end{bmatrix}, \quad (7)$$

system matrix

$$\mathbf{A}(z) = \begin{bmatrix} 0 & i\omega\rho(z) \\ -[i\omega\rho(z)]^{-1} K_z^2(z) & 0 \end{bmatrix} \quad (8)$$

and source vector

$$\mathbf{\Sigma}(z) = \begin{bmatrix} 0 \\ -i\omega I_v(z) \end{bmatrix}. \quad (9)$$

To characterize the difference between the reference and actual media, we introduce the velocity potential

$$\alpha_c(z) = 1 - \left( \frac{c_0}{c(z)} \right)^2 \quad (10)$$

and the density potential

$$\alpha_\rho(z) = \ln r_\rho(z), \quad r_\rho(z) = \frac{\rho_0}{\rho(z)}. \quad (11)$$

The vertical wavenumber can now be expressed as

$$K_z(z) = k_z \Gamma(z),$$

where

$$\Gamma(z) = \frac{K_z(z)}{k_z} = [1 - \kappa^2 \alpha_c(z)]^{\frac{1}{2}} \quad (12)$$

is a function of the velocity potential, but not frequency, and defines the ratio of the vertical wavenumbers in the actual and reference media.

In the scattering formalism, the system matrix can then be written as

$$\mathbf{A}(z) = \begin{bmatrix} 0 & i\omega\rho_0 r_\rho^{-1}(z) \\ -[i\omega\rho_0]^{-1} r_\rho(z) k_z^2 \Gamma^2(z) & 0 \end{bmatrix}. \quad (13)$$

The field vector  $\mathbf{B}$  can be decomposed into a wave vector  $\mathbf{W} = (U, D)^T$  containing upgoing ( $U$ ) and downgoing ( $D$ ) pressure waves by an eigensystem analysis of the system matrix  $\mathbf{A}$ . By inserting the eigenvectors of  $\mathbf{A}$  into the columns of the matrix  $\mathbf{L}$ , the up/down decomposition is achieved by the linear transformation

$$\mathbf{W} = \mathbf{L}^{-1} \mathbf{B}, \quad (14)$$

where

$$\mathbf{L}^{-1} = \frac{1}{2} \begin{bmatrix} 1 & -Z \\ 1 & Z \end{bmatrix} \quad (15)$$

is the decomposition matrix, and

$$\mathbf{L} = \begin{bmatrix} 1 & 1 \\ -Z^{-1} & Z^{-1} \end{bmatrix} \quad (16)$$

is the composition matrix, with

$$Z(z) = Z_0 [r_\rho(z) \Gamma(z)]^{-1},$$

where  $Z_0 = \rho_0 \omega / k_z$  is the acoustic impedance.

### 2.1. Differential equation for $\mathbf{W}$ in an inhomogeneous medium

Disregarding the source term in equation (6), the differential equation for  $\mathbf{W}$  in an inhomogeneous medium follows from equation (6) as

$$\frac{d\mathbf{W}(z)}{dz} = \left[ \mathbf{\Lambda}(z) - \mathbf{L}^{-1}(z) \frac{d\mathbf{L}(z)}{dz} \right] \mathbf{W}(z), \quad (17)$$

where the eigenvalue decomposition of  $\mathbf{A}$  gives the diagonal eigenvalue matrix

$$\mathbf{\Lambda} = \mathbf{L}^{-1} \mathbf{A} \mathbf{L}. \quad (18)$$

Equation (17) can then be written as

$$\frac{d\mathbf{W}(z)}{dz} = \begin{bmatrix} -ik_z \Gamma(z) & 0 \\ 0 & ik_z \Gamma(z) \end{bmatrix} \mathbf{W}(z) + s(z) \begin{bmatrix} 1 & -1 \\ -1 & 1 \end{bmatrix} \mathbf{W}(z), \quad (19)$$

where  $s$  is the scattering function:

$$s(z) = -\frac{1}{2} Z(z) \left( \frac{dZ^{-1}(z)}{dz} \right) = -\frac{1}{2} \frac{d}{dz} \ln [r_\rho(z) \Gamma(z)]. \quad (20)$$

The differential equations for  $U$  and  $D$  thus become

$$\frac{dU(z)}{dz} = -ik_z \Gamma(z) U(z) + s(z) [U(z) - D(z)] \quad (21)$$

and

$$\frac{dD(z)}{dz} = ik_z \Gamma(z) D(z) + s(z) [D(z) - U(z)]. \quad (22)$$

Note that the upgoing and downgoing waves are coupled because of the vertical variations of the medium parameters, which are expressed by the term  $dL/dz$ .

In the reference medium,  $\alpha_c = \alpha_\rho = 0$ , and the exact solutions for the upgoing and downgoing waves are

$$U(z) = \exp(-ik_z z) U(0), \quad D(z) = \exp(ik_z z) D(0).$$

Neither of these two solutions admit scattering.

As is usual in the scattering theory, the potentials  $\alpha_c(z)$  and  $\alpha_\rho(z)$  are assumed to vanish asymptotically, i.e.  $\alpha_c(z), \alpha_\rho(z) \rightarrow 0$  as  $z \rightarrow \pm\infty$ , at which limit the wavefunction  $P$  is merely a plane propagating wave described by  $\exp(\pm ik_z z)$ .

## 2.2. WKBJ solutions for incident and scattered waves

Equations (21) and (22) are general differential equations for  $U$  and  $D$ , respectively, and they describe all possible wave arrivals in the layered medium. In particular, they show how the entire wave field is made up of all the internal reflections and refractions within the medium. This wave field can be represented by an infinite series, known as the Bremmer series (Bremmer 1951), each term of which represents a wave that is reflected a particular number of times inside the medium.

In this paper, however, our interest is to describe single scattering. To this end, we must describe the downward propagation of the incident field and its interaction with the upward propagating single-scattered wave. Then, for the incident field we neglect the coupling of  $U$  with  $D$ . (We do not include the generation of downgoing waves (multiples) caused by the upgoing scattered field.) Disregarding this interaction, which is called the zero-order WKBJ approximation, gives the one-way wave equation for the incident field

$$\frac{dD_0(z)}{dz} = [ik_z \Gamma(z) + s(z)] D_0(z), \quad (23)$$

with solution

$$D_0(z) = D_0(0) \exp\left(\int_0^z dz' s(z')\right) \exp\left(ik_z \int_0^z dz' \Gamma(z')\right). \quad (24)$$

The boundary condition states that just below the source, the downgoing field is that radiated by the source:

$$D_0(0^+) = A(k) = -\frac{a(\omega)}{2ik_z}, \quad (25)$$

where  $a(\omega)$  is the source strength. By evaluating the integral over  $s$ , we obtain the following zero-order WKBJ solution for the downgoing field:

$$D_0(z) = A(k) [r_\rho(z) \Gamma(z)]^{-\frac{1}{2}} \exp\left(ik_z \int_0^z dz' \Gamma(z')\right). \quad (26)$$

It is convenient to characterize the phase of the incident field in terms of the difference between wave propagation in models without and with the influence of the velocity potential. Equation (26) can then be written as

$$D_0(z) = A(k) [r_\rho(z) \Gamma(z)]^{-\frac{1}{2}} \exp(ik_z [z - \xi(z)]), \quad (27)$$

where the WKBJ shift function

$$\xi = \xi_W(z) = \int_{-\infty}^z dz' [1 - \Gamma(z')] \quad (28)$$

now picks up the additional phase caused by the velocity potential. The WKBJ shift function obeys the differential equation

$$-2\xi'_W + (\xi'_W)^2 + \kappa^{-2}\alpha_c = 0, \quad \xi_W^{(n)} = 0, \quad n \geq 2, \quad (29)$$

which is straightforwardly verified by direct substitution. The zero of the second- and higher-order derivatives of the shift function implies that inside a layer it must vary slowly over a wavelength.

The scattered field is solved in the first-order WKBJ approximation, where the zero-order WKBJ approximation incident field (27) is substituted into the differential equation (21). The scattered field then satisfies the linear first-order differential equation

$$\frac{dU_1(z)}{dz} + [ik_z\Gamma(z) - s(z)]U_1(z) = -s(z)D_0(z). \quad (30)$$

Taking into account the radiation condition,  $U(\infty) = 0$  (no scattered (upgoing) waves at infinity), the solution for the scattered field at the measurement level is

$$U_1(z=0) = A(k) \int_0^\infty dz s(z) \exp(2ik_z[z - \xi(z)]). \quad (31)$$

Thus, the scattered field is an integral over all depths of the logarithmic derivative of an angle-weighted acoustic impedance ratio, retarded by two-way traveltimes.

### 2.3. The single-scattering forward model

It is convenient to express the single-scattering data in terms of the dimensionless scattering amplitude  $\Phi = A^{-1}U_1$ . Our objective is to analyse the logarithmic changes of the acoustic potentials and not their vertical derivatives as expressed by the scattering function  $s$  in equation (20). A partial integration in equation (31) leads to the following result for the dimensionless scattering amplitude:

$$\Phi(k) = -\frac{ik}{2\kappa} \int_0^\infty dz \alpha(z) \exp(2ik_z[z - \xi(z)]), \quad (32)$$

where  $\alpha(z)$  is an angle-dependent scattering potential:

$$\alpha(z) = -2 \ln[r_\rho(z)\Gamma(z)]\Gamma(z). \quad (33)$$

Equation (32) is a nonlinear forward model for computing the dimensionless scattering amplitude  $\Phi(k)$  from the potential  $\alpha$ . We make the following remarks. The single scattering amplitude is found by performing an integral over depth over the product of an amplitude function and a delay function. The amplitude function is the scattering potential. The delay function consists of the product of two functions, where the first  $\exp(2ik_z z)$  accounts for the two-way wave propagation of the unperturbed wave in the reference medium, whereas the second  $\exp[-2ik_z \xi(z)]$  corrects for the influence of the potential. Since the scattered wave  $U_1(z)$  travels through the same potential  $\alpha(z)$  as the incident wave  $D_0(z)$ , the shift function  $\xi(z)$  is the same for both cases. For a piecewise-constant layered medium, the delay function in the WKBJ approximation predicts the exact traveltimes of the single scattering events. However, performing the integral over depth, the predicted amplitudes of the single scattering events will not be exact for the piecewise-constant layered medium unless the boundary conditions of continuity of the pressure and the vertical component of the particle velocity at the interfaces

are explicitly introduced. For the sake of forward modelling, the boundary conditions can easily be accounted for. Interfaces or discontinuities in the potential are then treated by correctly coupling the incident wave to the scattered waves. However, for the inverse problem, where the location of interfaces is not known, it would be cumbersome to account for the continuity conditions in an explicit manner. Therefore, we choose to neglect these conditions at the expense of using a forward model that predicts slightly incorrect amplitudes of the single scattering events.

When we later simulate data to test the inverse scattering algorithm to be described in the following section, we do not base the simulation on the single scattering forward model (32), but on the exact forward model for primary reflections in a piecewise-constant layered medium. This model is described in appendix A.

*2.3.1. The eikonal approximation* The eikonal approximation is based upon an expansion of the square root in the WKBJ shift function (28) to first order in the dimensionless potential  $\alpha_c$ . The shift function entering the forward model (32) in the eikonal approximation is then

$$\xi = \xi_E(z) = \frac{1}{2\kappa^2} \int_{-\infty}^z dz' \alpha_c(z'). \quad (34)$$

The eikonal approximation implies a weak velocity potential assumption, where the vertical wavenumber ratio  $\Gamma$  in equation (12) is

$$\Gamma(z) \approx \Gamma_E(z) = 1 - \frac{\kappa^2}{2} \alpha_c(z). \quad (35)$$

The eikonal approximation is not discussed further in the present paper.

*2.3.2. The Born approximation.* By the expression ‘Born approximation’, it is understood that the exact incident wave is replaced by the unperturbed incident wave  $\exp(ik_z z)$ . In the forward model developed in this paper, the Born approximation translates to setting the shift function in the forward model (31) to zero:

$$\xi = \xi_B(z) \equiv 0. \quad (36)$$

The dimensionless scattering amplitude in the Born approximation becomes

$$\Phi_B(k) = -\frac{ik}{2\kappa} \int_0^\infty dz \alpha(z) \exp(2ik_z z), \quad (37)$$

with the angle-dependent scattering potential

$$\alpha(z) = -2 \ln[r_\rho(z)\Gamma(z)]. \quad (38)$$

Appendix B discusses the relationship between the Born potential and the primary reflection response.

### 3. Inverse scattering

The forward problem associated with equation (32) is stated as follows. Given the velocity and density potentials  $\alpha_c$  and  $\alpha_\rho$  (or equivalently, the velocity and density ratios), respectively, find the dimensionless scattering amplitude  $\Phi$  that satisfies the prescribed boundary conditions. In this section, we develop a procedure for reconstructing the velocity and density potentials from the dimensionless scattering amplitude  $\Phi$ . The solution is obtained in three steps. First, the angle-dependent Born potential  $\alpha_B$  is computed by migrating the single scattering events in the time intercept-slowness domain by using a constant reference medium. Second, we show

that squeezed velocity and density potentials  $\hat{\alpha}_c$  and  $\hat{\alpha}_\rho$ , respectively, can be estimated by AVA inversion of the residual moveout-corrected Born potential. Third, we show how the squeezed potentials can be depth corrected by applying a nonlinear stretch function. The three steps which require no information about the subsurface parameters except the reference medium parameters can be described by the seismic data processing sequence constant-velocity (partial) migration–inversion–residual migration.

### 3.1. The angle-dependent Born potential and the single scattering data

As shown in appendix C, the inverse Fourier transform over the frequency of equation (32) yields

$$4 \int_{-\infty}^{2z/v_0} dt' \Phi(t') = \sum_{n=0}^{\infty} \frac{1}{n!} \frac{d^n}{dz^n} \alpha(z) \xi^n(z), \quad (39)$$

where  $z = v_0 t/2$ , and  $v_0 = c_0/\cos\theta$  is the plane-wave apparent velocity in the reference medium along the depth axis. Recall that in the Born approximation, the shift function is zero. By considering  $\xi = 0$  in the forward model (31), the single scattering Born potential, per definition, is obtained:

$$\alpha_B(z) \equiv \alpha(z)|_{\xi=0} = 4 \int_{-\infty}^{2z/v_0} dt' \Phi(t'). \quad (40)$$

Equation (40), which is a key equation in the inversion procedure, is known as constant-velocity migration or linear migration–inversion. Primary reflection events are placed at depths computed linearly using their traveltimes together with the constant reference velocity. Equation (39) can now be written as

$$\alpha_B(z) = \sum_{n=0}^{\infty} \frac{1}{n!} \frac{d^n}{dz^n} \alpha(z) \xi^n(z). \quad (41)$$

By neglecting terms  $d^n \xi/dz^n$  for  $n = 2, \dots, \infty$ , we can write equation (41) as an infinite sum where the  $n$ th term is proportional to the  $n$ th power of the derivative of the shift function

$$\alpha_B(z) \approx \sum_{n=0}^{\infty} \left( \frac{d\xi(z)}{dz} \right)^n \sum_{m=n}^{\infty} \frac{1}{(m-n)!} \binom{m}{n} \xi^{m-n}(z) \frac{d^{m-n} \alpha(z)}{dz^{m-n}}. \quad (42)$$

From the Born potential  $\alpha_B(z)$ , our goal is to use equation (42) as the basis for solving the inverse scattering problem.

### 3.2. Nonlinear AVA inversion: estimation of squeezed potentials $\hat{\alpha}_c$ and $\hat{\alpha}_\rho$ from $\alpha_B$

We now show that we can predict what the velocity and density layer potentials are, not as a function of their true depth, but as a function of the interface depths provided by the Born potential at a zero incidence angle. These potentials which are predicted from  $\alpha_B$  at two different angles are called ‘squeezed’ velocity and density potentials, denoted by  $\hat{\alpha}_c$  and  $\hat{\alpha}_\rho$ , respectively, because they mimic the potentials that would be obtained by compressing or squeezing the depth axis of the actual velocity and density potentials.

Before we proceed we make one remark. After constant-velocity imaging of the scattered data, one obtains one Born depth profile for every selected angle (or slowness). The first interface is always lined up at the correct depth, say  $z_1$ , in every Born depth profile. (The first primary travels in the known reference medium only.) The second and following interfaces will show some residual moveout across the Born depth profiles. Since we aim at predicting

the squeezed potentials  $\hat{\alpha}_c$  and  $\hat{\alpha}_\rho$  as a function of vertical depth from  $\alpha_B$  at minimum two different angles, the interface residual moveout must be corrected before the prediction can be done. The residual-moveout correction does not affect the variation in amplitude with respect to the angle of the Born potential.

Inside a layer, velocities are assumed to be constant (or vary smoothly with depth). It is then reasonable to disregard in equation (42) all derivatives of  $\alpha$ . The non-zero terms in equation (42) arrive for  $n = m$ , giving

$$\alpha_B(z) \approx \hat{\alpha}(z) \sum_{n=0}^{\infty} [1 - (1 - \kappa^2 \hat{\alpha}_c(z))^{\frac{1}{2}}]^n, \quad \frac{d^{n+1} \alpha(z)}{dz^{n+1}} = 0. \quad (43)$$

The sum is a geometric series, and we obtain

$$\alpha_B(z) \approx \frac{\hat{\alpha}(z)}{[1 - \kappa^2 \hat{\alpha}_c(z)]^{\frac{1}{2}}}. \quad (44)$$

By inserting equation (33) for  $\hat{\alpha}(z)$ , that is,  $\hat{\alpha}(z) = -2 \ln[\hat{r}_\rho(z) \hat{\Gamma}(z)] \hat{\Gamma}(z)$ , and recalling that  $\alpha_B$  is a function of angle  $\theta$ , we find

$$\alpha_B(\theta, z) = -2 \ln(\hat{r}_\rho(z) [1 - \sec^2 \theta \hat{\alpha}_c(z)]^{\frac{1}{2}}). \quad (45)$$

We make two comments. First, the relation between the Born potential and the squeezed velocity and density potentials is ‘exact’ within the limitations of the forward model which slightly mispredicts the amplitudes of the single-scattering events due to the neglect of the continuity of pressure and vertical component of particle velocity at layer interfaces. Further, the relation is nonlinear; it is not linearized in any way with respect to changes in the acoustic parameters as is commonly done in seismic amplitude versus angle analysis. Second, the relationship has not been derived by assuming that the single scattering is from a smoothly changing medium. Interfaces with step discontinuities in the medium parameters can be (and is) present. Thus, there is no requirement of small contrasts in the acoustic parameters across the interfaces. Therefore, relation (45) is the ticket to determining the acoustic parameters.

In addition to being useful, equation (45) is also simple and understandable, in particular when we rewrite it in terms of angle, and velocity and density changes. One obtains

$$\alpha_B(\theta, z) = -\ln \left[ \frac{1}{\cos^2 \theta} \left( \frac{\rho_0 c_0}{\rho(z) c(z)} \right) + \left( \frac{\rho_0}{\rho(z)} \right)^2 \sin^2 \theta \right]. \quad (46)$$

For small angles, we note that one can only hope to recover the acoustic impedance, which is a well-known result and no surprise. Larger angles are required to recover density.

We now proceed to find the scheme to estimate layer and density potentials. From equation (45), it follows that

$$\hat{r}_\rho^2(z) [1 - \sec^2 \theta \hat{\alpha}_c(z)] = \exp[-\alpha_B(\theta, z)]. \quad (47)$$

When the Born depth profile is known for two angles  $\theta_0$  and  $\theta_1$ , we can solve for the squeezed velocity potential

$$\hat{\alpha}_c(z) = \frac{\cos^2(\theta_1) - b(\theta_0, \theta_1, z) \cos^2(\theta_0)}{1 - b(\theta_0, \theta_1, z)}, \quad (48)$$

where

$$b = b(\theta_0, \theta_1, z) = \left( \frac{\cos \theta_1}{\cos \theta_0} \right)^2 \exp[\alpha_B(\theta_0, z) - \alpha_B(\theta_1, z)]. \quad (49)$$

From the estimated squeezed velocity potential and the calculated Born potential, the density ratio can be straightforwardly computed as

$$\frac{\hat{\rho}(z)}{\rho_0} = \hat{r}_\rho^{-1}(z) = [1 - \sec^2 \theta \hat{\alpha}_c(z)]^{\frac{1}{2}} \exp \left[ \frac{1}{2} \alpha_B(\theta, z) \right]. \quad (50)$$

### 3.3. Residual depth imaging: stretching of the squeezed potentials towards the actual potentials

For the 1D inverse scattering problem, Amundsen *et al* (2005a, 2005b) have shown how the squeezed velocity potential can be nonlinearly stretched with respect to the depth axis so that the potential discontinuities are moved towards their correct location. The nonlinear stretch function is a function of the squeezed velocity potential. Therefore, the solution is data driven in the respect that no information about the medium other than the squeezed velocity potential is required.

In the present case, two potentials have been estimated: the squeezed velocity potential and the squeezed density potential. The data-driven depth imaging step, however, is similar to that in the 1D case. The only difference is that in the present case the additional density potential must be stretched. The stretch function for both potentials is the same and depends solely on the squeezed velocity potential.

Equation (42) is a basis for deriving a closed-form solution for  $\alpha$ . To this end, the Fourier representation of  $\alpha(z)$  is introduced, which gives

$$\alpha_B(z) \approx \sum_{n=0}^{\infty} \left( \frac{d\xi(z)}{dz} \right)^n \frac{1}{2\pi} \int_{-\infty}^{\infty} dk D_n(k\xi) \exp(-ikz) \alpha(k), \quad (51)$$

where

$$D_n(k\xi) = \sum_{m=n}^{\infty} \frac{1}{(m-n)!} \binom{m}{n} [-ik\xi(z)]^{m-n}. \quad (52)$$

The sum  $D_n$  can be written as

$$D_n(k\xi) = \exp[-ik\xi(z)] \sum_{m=0}^n \frac{1}{m!} \binom{n}{m} [-ik\xi(z)]^{n-m}, \quad (53)$$

and the expression for the Born potential then becomes

$$\alpha_B(z) \approx \frac{1}{2\pi} \int_{-\infty}^{\infty} dk \left\{ \sum_{n=0}^{\infty} \left( \frac{d\xi(z)}{dz} \right)^n \sum_{m=0}^n \frac{1}{m!} \binom{n}{m} [-ik\xi(z)]^{n-m} \right\} \exp[-ik(z + \xi(z))] \alpha(k). \quad (54)$$

In equation (54), the double sum can be written as a single sum that is recognized as an expression for the exponential function

$$\begin{aligned} \sum_{n=0}^{\infty} \left( \frac{d\xi(z)}{dz} \right)^n \sum_{m=0}^n \frac{1}{m!} \binom{n}{m} [-ik\xi(z)]^{n-m} &= \frac{1}{1 - \xi'(z)} \sum_{n=0}^{\infty} \frac{(-1)^n}{n!} \left( \frac{ik\xi(z)\xi'(z)}{1 - \xi'(z)} \right)^n \\ &= \frac{1}{1 - \xi'(z)} \exp\left( -\frac{ik\xi(z)\xi'(z)}{1 - \xi'(z)} \right). \end{aligned} \quad (55)$$

The Born potential in equation (54) now reads

$$\alpha_B(z) \approx \left( 1 - \frac{d\xi(z)}{dz} \right)^{-1} \frac{1}{2\pi} \int_{-\infty}^{\infty} dk \exp\left[ -ik \left( z + \frac{\xi(z)}{1 - \xi'(z)} \right) \right] \alpha(k). \quad (56)$$

Using the translation property of the Fourier transform, we obtain a closed-form expression for the Born potential

$$\alpha_B(z) \approx \left( 1 - \frac{d\xi(z)}{dz} \right)^{-1} \alpha \left( z + \frac{\xi(z)}{1 - \frac{d\xi(z)}{dz}} \right). \quad (57)$$

As shown for the 1D scattering case by Amundsen *et al* (2005b), equation (57) can be improved by introducing two new approximations, both of which are valid in the WKB approximation. First, under the WKB assumption, when  $\xi''(z)$  is negligible, the replacement

$$\frac{\xi(z)}{1 - \frac{d\xi(z)}{dz}} \rightarrow \int_{-\infty}^z dz' \frac{\frac{d\xi(z')}{dz'}}{1 - \frac{d\xi(z')}{dz'}}, \quad \xi''(z) = 0, \quad (58)$$

is justified. Second, when  $\xi''(z)$  and all higher-order derivatives are disregarded, the following replacement is justified:

$$[1 - \kappa^2 \alpha_c(z)]^{-\frac{1}{2}} \rightarrow [1 - \kappa^2 \hat{\alpha}_c(z)]^{-\frac{1}{2}}, \quad \frac{d^n \xi(z)}{dz^n} = 0, \quad n \geq 2. \quad (59)$$

Inserting the two approximations into equation (57) and recalling equation (28) give the result

$$\alpha_B(z) \approx [1 - \kappa^2 \hat{\alpha}_c(z)]^{-\frac{1}{2}} \alpha \left( z + \int_{-\infty}^z dz' [(1 - \kappa^2 \hat{\alpha}_c(z'))^{-\frac{1}{2}} - 1] \right). \quad (60)$$

By using relationship (44) between the Born potential  $\alpha_B$  and the squeezed potential  $\hat{\alpha}$ , equation (60) can be rewritten in the following form:

$$\hat{\alpha}(z) = \alpha \left( z + \int_{-\infty}^z dz' [(1 - \kappa^2 \hat{\alpha}_c(z'))^{-\frac{1}{2}} - 1] \right). \quad (61)$$

The nonlinear AVA inversion has determined the squeezed velocity and density potentials,  $\hat{\alpha}_c$  and  $\hat{\alpha}_\rho$ , respectively. On the other hand, equation (61) gives the depth imaging procedure to obtain the full angle-dependent potential. However, since both  $\hat{\alpha}$  and  $\alpha$  show the same dependency upon their respective velocity and density potentials, as well as angle, depth imaging of the velocity and density potentials must obey the same formula, respectively,

$$\hat{\alpha}_c(z) = \alpha_c \left( z + \int_{-\infty}^z dz' [(1 - \hat{\alpha}_c(z'))^{-\frac{1}{2}} - 1] \right) \quad (62)$$

and

$$\hat{\alpha}_\rho(z) = \alpha_\rho \left( z + \int_{-\infty}^z dz' [(1 - \hat{\alpha}_c(z'))^{-\frac{1}{2}} - 1] \right). \quad (63)$$

Thus, provided that the Born potential has been computed according to equation (40), (62) and (63) suggest a two-step procedure for estimating the velocity and density potentials. First, the squeezed velocity and density potentials  $\hat{\alpha}_c$  and  $\hat{\alpha}_\rho$ , respectively, are estimated by the nonlinear AVA inversion of the Born potential. Then, the actual velocity and density potentials  $\alpha_c$  and  $\alpha_\rho$  are derived by applying a nonlinear shift to  $\hat{\alpha}_c$  and  $\hat{\alpha}_\rho$  according to equations (62) and (63), respectively. The nonlinear shift is seen to correspond to stretching the depth axis of the squeezed potentials. The effect of stretching is to locate interfaces that are mislocated in  $\hat{\alpha}_c$  and  $\hat{\alpha}_\rho$  towards their correct location. Thus, in the absence of the actual velocity function, the nonlinear AVA analysis and depth imaging (stretch) algorithm extract the necessary information solely from the angle-dependent Born depth profile  $\alpha_B(z)$ .

Finally, we remark that the residual depth imaging can be applied directly to the squeezed velocity and density profiles as

$$\hat{c}(z) = c \left( z + \int_{-\infty}^z dz' [(1 - \hat{\alpha}_c(z'))^{-\frac{1}{2}} - 1] \right) = c \left( c_0^{-1} \int_{-\infty}^z dz' \hat{c}(z') \right) \quad (64)$$

and

$$\hat{\rho}(z) = \rho \left( z + \int_{-\infty}^z dz' [(1 - \hat{\alpha}_c(z'))^{-\frac{1}{2}} - 1] \right) = \rho \left( c_0^{-1} \int_{-\infty}^z dz' \hat{c}(z') \right), \quad (65)$$

where  $\hat{c}$  is the squeezed velocity profile defined through the squeezed velocity potential.

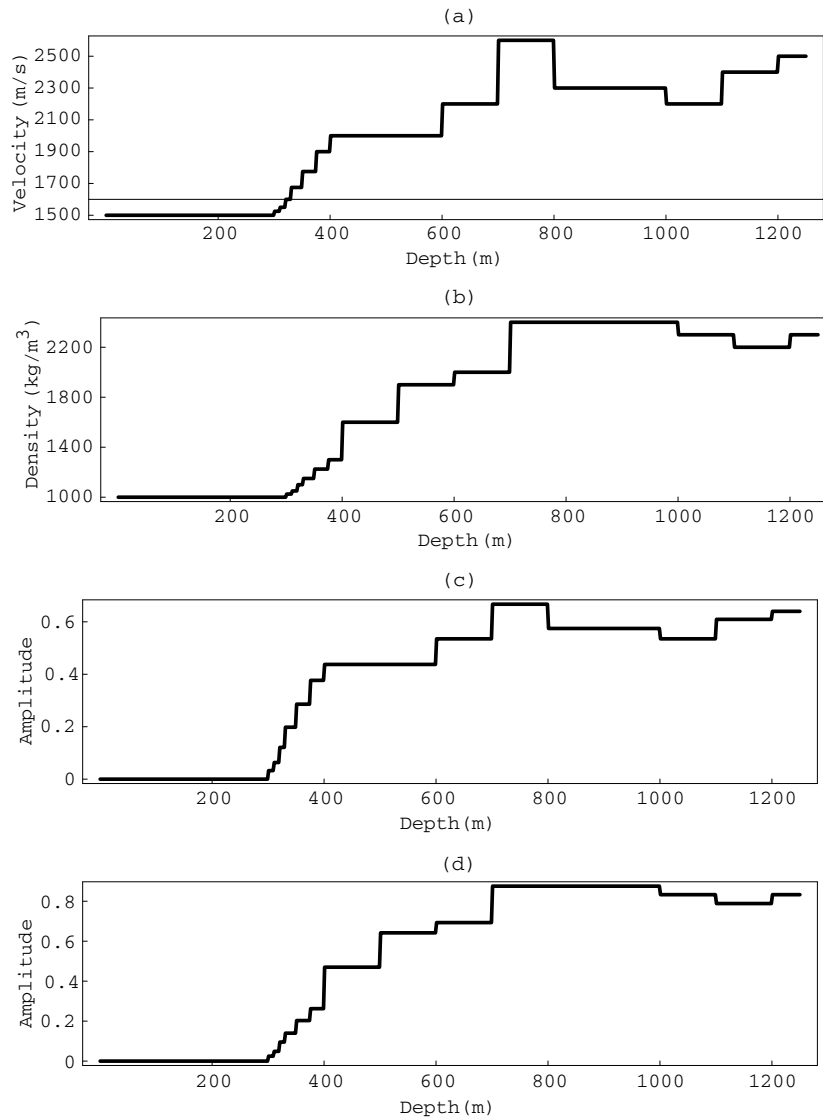


**Figure 1.** Actual models: (a) velocity,  $c(z)$ ; (b) density,  $\rho(z)$ ; (c) velocity potential,  $\alpha_c(z)$  and (d) negative of density potential,  $\alpha_\rho(z)$ . The model is listed in table 1.

#### 4. Model calculations

As an example of the nonlinear direct AVA analysis and data-driven depth imaging with the objective to estimate the depth-dependent velocity and density potentials, and related velocity and density, from the single scattering data, we consider the high-velocity/high-density contrast piecewise-constant fifteen-layer acoustic medium, as displayed in figure 1 and listed in table 1. The reference velocity and density (in layer zero) are  $c_0 = 1500 \text{ m s}^{-1}$  and  $\rho_0 = 1000 \text{ kg m}^{-3}$ , respectively. The model has some properties that should be noted. The velocity is constant in layers 8 and 9, whereas the density is constant in layers 11 and 12. In addition, there is a velocity increase, but a density decrease between layers 13 and 14.

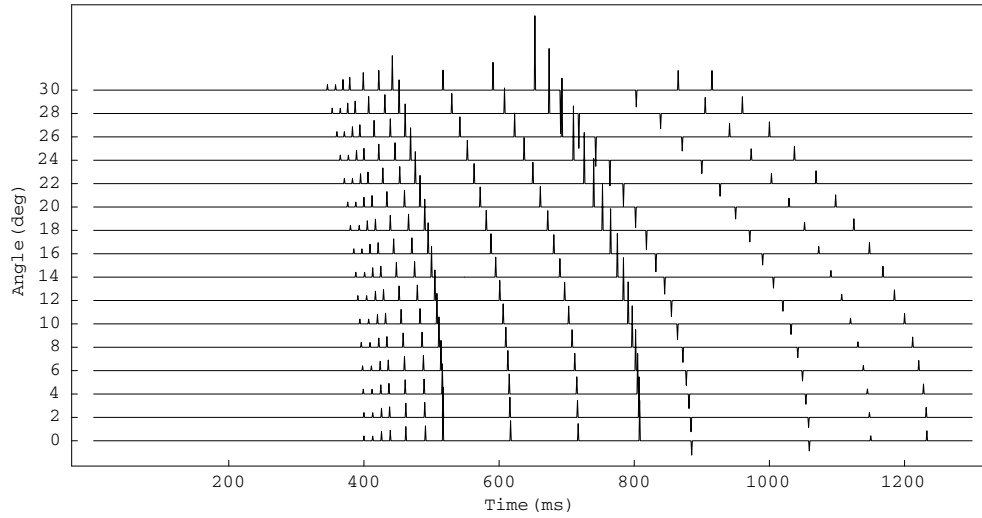


**Figure 2.** Angle gather of primary reflection events as a function of time intercept from the fifteen-layer (fourteen-interface) model in figure 1. The eight reflection does not show amplitude variation with angle, consistent with a density contrast only between layers 8 and 9. The angles are defined in terms of the reference velocity as in equation (5).

**Table 1.** Fifteen-layer model, with reference velocity  $c_0 = 1500 \text{ m s}^{-1}$  and density  $\rho_0 = 1000 \text{ kg m}^{-3}$ . Here,  $z_n$  is the actual layer depth,  $z_{nB}(0)$  is the layer depth from zero-angle Born constant-velocity migration,  $\hat{z}_n$  is the estimated actual layer depth,  $c_n$  is the actual layer velocity,  $\hat{c}_n$  is the estimated layer velocity,  $\varepsilon_{c_n}$  is the relative error of the layer velocity estimate,  $\rho_n$  is the actual layer density,  $\hat{\rho}_n$  is the estimated layer density,  $\varepsilon_{\rho_n}$  is the relative error of the layer density estimate,  $\alpha_{c_n}$  is the actual velocity potential,  $\alpha_{\rho_n}$  is the actual density potential and  $R_n(0)$  is the zero-angle reflection coefficient.

$n$	$z_n$ (m)	$z_{nB}$ (0)(m)	$\hat{z}_n$ (m)	$c_n$ (m s <sup>-1</sup> )	$\hat{c}_n$ (m s <sup>-1</sup> )	$\varepsilon_{c_n}$ (%)	$\rho_n$ (kg m <sup>-3</sup> )	$\hat{\rho}_n$ (kg m <sup>-3</sup> )	$\varepsilon_{\rho_n}$ (%)	$\alpha_{c_n}$	$\alpha_{\rho_n}$	$R_n(0)$
0				1500			1000			0	0	
1	300	300	300	1525	1525	0.0	1025	1025	0.0	0.03	-0.02	0.021
2	310	309.8	310	1550	1550	0.0	1050	1050	0.0	0.06	-0.05	0.020
3	320	319.5	320	1600	1600	0.0	1100	1100	0.0	0.12	-0.10	0.039
4	330	328.9	330	1675	1674	0.1	1150	1150	0.0	0.20	-0.14	0.045
5	350	346.8	350	1775	1773	0.1	1225	1225	0.0	0.29	-0.20	0.061
6	375	367.9	375	1900	1895	0.3	1300	1301	0.0	0.38	-0.26	0.064
7	400	387.7	400	2000	1988	0.6	1600	1599	0.1	0.44	-0.47	0.129
8	500	462.7	500	2000	1983	0.9	1900	1894	0.3	0.44	-0.64	0.086
9	600	537.7	599	2200	2173	1.2	2000	1990	0.5	0.54	-0.69	0.073
10	700	605.8	698	2600	2541	2.3	2400	2371	1.2	0.67	-0.88	0.173
11	800	663.5	795	2300	2272	1.2	2400	2366	1.4	0.57	-0.88	-0.061
12	1000	794.0	992	2200	2193	0.3	2300	2262	1.7	0.54	-0.83	-0.043
13	1100	862.2	1093	2400	2370	1.3	2200	2177	1.1	0.61	-0.79	0.021
14	1200	924.7	1191	2500	2451	1.9	2300	2277	1.0	0.64	-0.83	0.043

In the example, data are modelled in the time intercept-slowness domain with the algorithm described in appendix A. The primary reflection data from the model are plotted in figure 2 as traces as a function of angle, ranging from 0 to 30°, for an infinite bandwidth. The related

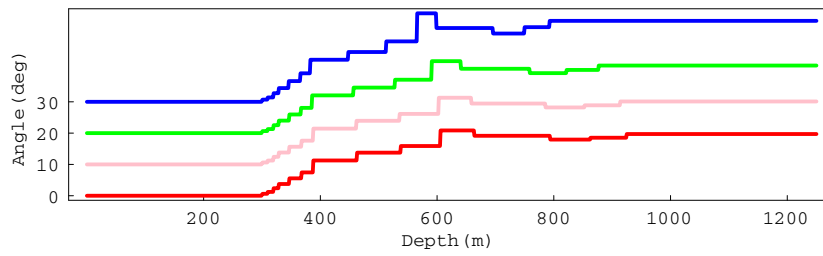


**Figure 3.** Angle gather of Born potential depth profiles. The red, pink, green and blue colours represent angles of 0, 10, 20 and 30°, respectively. The angles are defined in terms of the reference velocity as in equation (5).

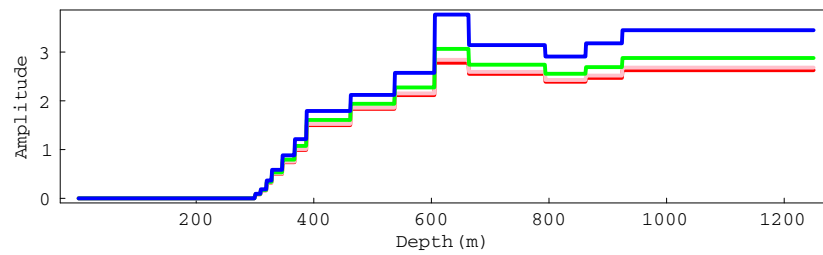


**Figure 4.** Moveout-corrected angle gather of Born potential depth profiles corresponding to the gather in figure 3. The red, pink, green and blue colours represent angles of 0, 10, 20 and 30°, respectively. The angles are defined in terms of the reference velocity as in equation (5).

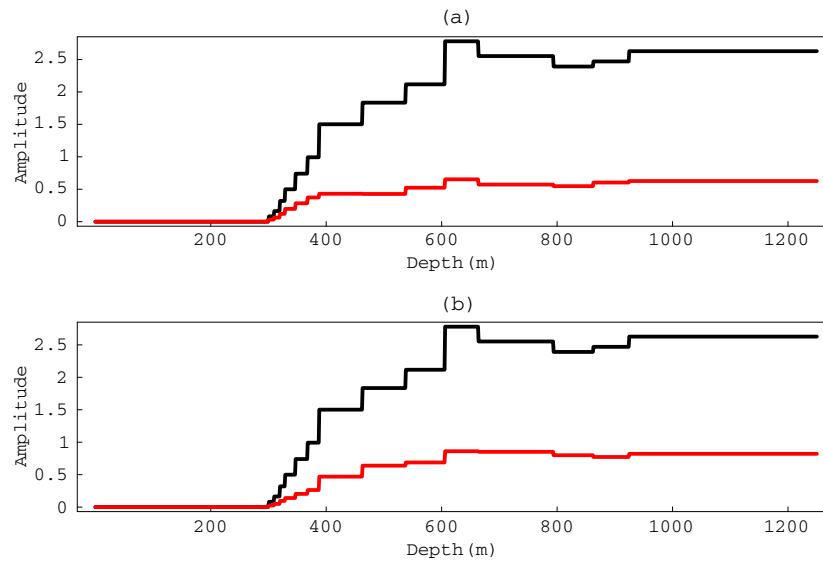


**Figure 5.** Nonlinear AVA analysis of the moveout-corrected angle-dependent Born potential (at 0 and 20 degrees; see figure 4) gives squeezed potentials (red lines): (a) velocity potential and (b) negative of density potential. For comparison, the zero-angle Born potential profile is displayed as a black line.

angle-dependent Born potential is obtained by constant-velocity migration of each of the angle traces. Figure 3 shows a selection of the Born potential depth profiles for angles of 0, 10,

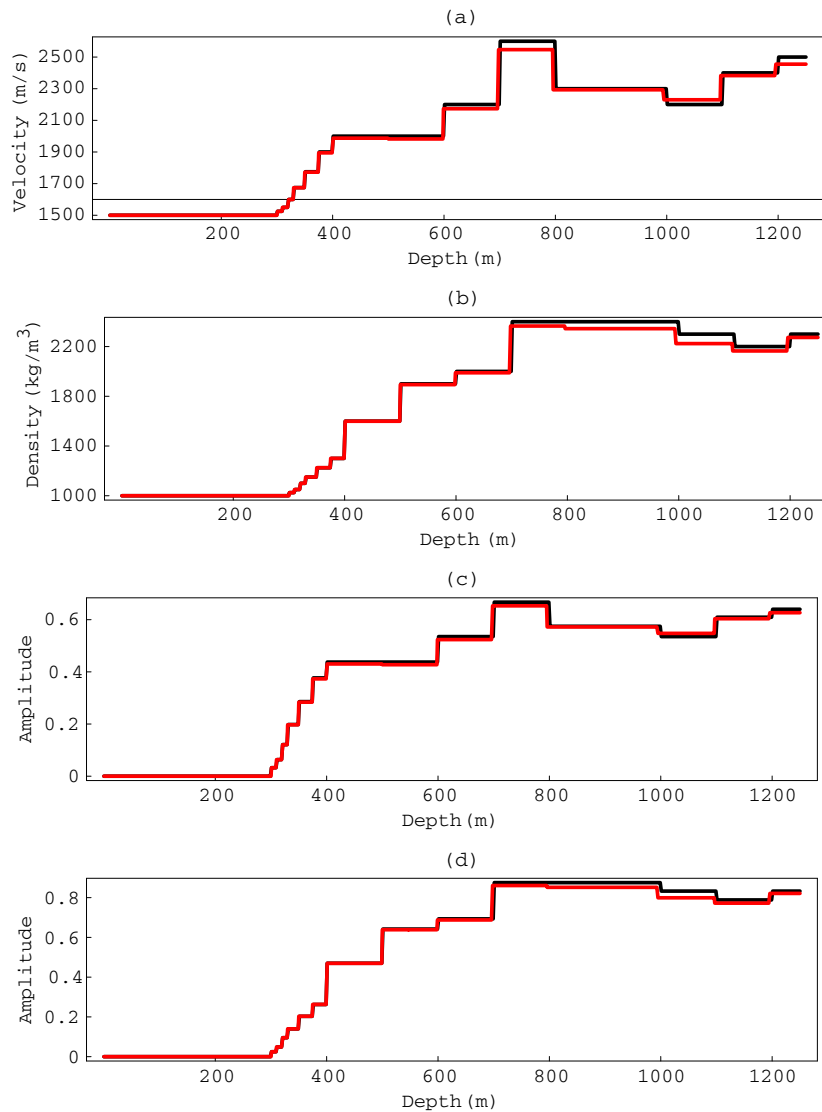


**Figure 6.** Data-driven depth imaging. Medium parameters are obtained by stretching the squeezed potentials displayed in figure 5: (a) estimated velocity, (b) estimated density, (c) estimated velocity potential and (d) negative of the estimated density potential. The estimated curves are shown in red lines. For comparison, the actual models are displayed in black lines.

20 and 30°. Observe that the first interface is correctly positioned in depth (at  $z_1 = 300$  m) in all the angle profiles since the primary from the first interface always propagates with the reference velocity. The other interfaces are generally severely mislocated in depth. In addition, the image depth of these interfaces varies with angle, in the predictable way that the depth decreases with an increasing angle. We call this behaviour the interface residual moveout. Before any AVA analysis, the interface residual moveout should be corrected so that all Born depth profiles have interface depths matching the interface depths of the zero-angle Born depth profile. Since the number of interfaces is the same in every Born depth profile, the residual

moveout correction to apply can be easily found, for instance, by applying edge-detection techniques to each individual profile. Figure 4 shows the residual moveout-corrected angle gather of the Born potential depth profiles corresponding to the gather in figure 3. In the figure 4 gather, the interfaces are positioned at the same depth, but still the amplitudes of the residual moveout-corrected Born profiles differ as a function of the angle. The amplitude variation versus angle is the basis for estimating the squeezed depth-dependent velocity and density potentials. In the present study, we use only the moveout-corrected angle-Born profiles at 0 and 20° to estimate the squeezed potentials. Figure 5 displays the squeezed velocity and density potentials. For comparison, the zero-angle Born potential profile is shown in the same figure. Evidently, the depth of the interfaces of the squeezed potentials and the zero-angle Born profile matches. From the squeezed layer potentials, estimates of layer velocity and density,  $\hat{c}_n$  and  $\hat{\rho}_n$ , respectively, can be found. Observe that the estimated velocity and density, presented in table 1 together with the actual velocity and density  $c_n$  and  $\rho_n$ , respectively, display the same properties as the true parameters. The estimated layer velocity and density are at maximum approximately 2% off.

From the squeezed potentials, the actual velocity and density potentials can be estimated in the WKB approximation by data-driven depth imaging, amounting to stretching the depth axis of the squeezed potentials using the amplitude of the squeezed velocity potential only. The results, both for velocity and density and related potentials, are shown in figure 6. The estimated interface depth  $\hat{z}_n$  is summarized in table 1.

## 5. Conclusions

We have given the forward model for acoustic single scattering from a depth-variable acoustic medium in the WKB, eikonal and Born approximations. We have shown that the acoustic inverse scattering problem can be solved in three main steps. First, from the single scattering data in the time intercept-slowness domain, an angle-dependent Born potential profile is computed by constant-velocity imaging. Second, from the angle-dependent residual moveout-corrected Born potential depth profiles, nonlinear direct AVA analysis is used to estimate depth-dependent squeezed velocity and density potentials. The squeezed actual potentials contain information of the amplitude of the corresponding actual potentials, not within the actual potential layer interfaces, but within the layer interfaces of the zero-angle profile of the Born potential. Third, the mislocated reflectors in the squeezed potentials are moved with high precision towards their correct spatial location by applying a nonlinear stretch function. The nonlinear AVA analysis and data-driven depth imaging require no information of the medium other than the angle-dependent Born potential. In the nomenclature of seismic data processing, the three steps can be described by the sequence constant-velocity (partial) migration—inversion—residual migration.

A simple model example showed how the velocity and density potentials with associated velocities and densities could be estimated in the WKB approximation, from the angle-dependent Born potential. Even for high-velocity and high-density contrast media (strong potentials), the theory gives an inverse scattering procedure that reconstructs the potentials and their nature to a good approximation.

## Acknowledgments

We thank Statoil ASA for allowing us to publish this work. The first author (LA) would like to thank Professor Arthur B Weglein for sharing his visions, knowledge and deep understanding

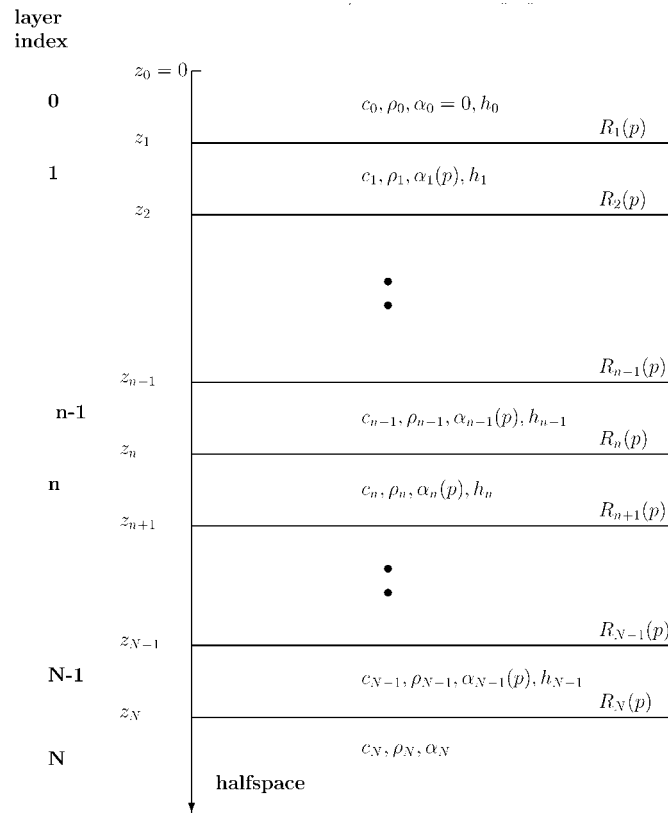


**Figure A1.** Layered medium. The velocity  $c(z)$ , density  $\rho(z)$  and potential  $\alpha(z)$  are generally discontinuous at layer interfaces  $z_1, z_2, \dots, z_N$ .

on the inverse scattering topic, which has benefited the current work. Further, he thanks Kris Innanen, Simon Shaw and Haiyan Zhang for providing keen insights on their work on the inverse scattering series.

### Appendix A. Modelling of the primary reflection response

We consider plane-wave propagation with slowness (ray parameter)  $p = \sin \theta / c_0$  through a medium with  $N + 1$  homogeneous layers with constant layer velocities  $c_n$ , densities  $\rho_n$  and thicknesses  $h_n$  as shown in figure A1. The source and receiver are both located at depth  $z = 0$  in the zeroth layer which is the reference medium with velocity  $c_0$  and density  $\rho_0$ .

The differential equations (21) and (22) together with proper boundary conditions show that the pressure field is made up of an infinite sum of reflections and refractions inside the medium (cf Bremmer (1951) and Santos *et al* (1996)). In what follows we show how to model the primary reflection response, that is, the waves that are split off by reflection from the downgoing source wavefield when it is transmitted into the medium. To this end, it is necessary to define the reflection and transmission coefficients in the stack of layers. As is well known, the coefficients can be derived by assuming that the pressure and the vertical particle velocity are continuous fields at every boundary. For a plane wave incident in layer

$n - 1$ , the reflection coefficient is

$$R_n(p) = \frac{\rho_n v_n(p) - \rho_{n-1} v_{n-1}(p)}{\rho_n v_n(p) + \rho_{n-1} v_{n-1}(p)}, \quad (\text{A.1})$$

where

$$v_n(p) = \frac{c_n}{\sqrt{1 - (c_n p)^2}}$$

is the apparent velocity in layer  $n$  along the depth axis, and the transmission coefficient is

$$T_n^{(D)}(p) = 1 + R_n(p).$$

We will also require that a wave transmitted in the opposite direction, upwards from layer  $n$  into layer  $n - 1$ , has the transmission coefficient

$$T_n^{(U)}(p) = 1 - R_n(p).$$

Thus, the two-way transmission loss for a plane wave passing down and up through the interface at depth  $z_n$  is

$$T_n^{(D)}(p)T_n^{(U)}(p) = 1 - R_n^2(p).$$

When the source is initiated with unit strength, a plane wave propagates downwards with velocity  $c_0$  into the discontinuous, layered medium. At the boundary of the first layer, at depth  $z_1 = h_0$ , the incident wave which is represented by

$$D_0(\omega, p) = \exp[i\omega h_0/v_0(p)],$$

is split into [I] a refracted wave penetrating into this layer with amplitude  $T_1^{(D)}(p)$  and represented by

$$D_1(\omega, p) = D_0(\omega, p)T_1^{(D)}(p) \exp[i\omega(z - z_1)/v_1(p)], \quad z_1 < z < z_2,$$

and [II] a reflected wave with amplitude  $R_1(p)$  returning to the receiver level where it is represented by

$$\Phi_1(\omega, p) = R_1(p) \exp[2i\omega h_0/v_0(p)].$$

The downgoing wave  $D_1(\omega, p)$  will be split at the next interface at depth  $z_2$  into a refracted wave

$$D_2(\omega, p) = D_1(\omega, p)T_2^{(D)}(p) \exp[i\omega(z - z_2)/v_2(p)], \quad z_2 < z < z_3,$$

penetrating into layer 3, and a reflected wave which, after being refracted through the interface at depth  $z_1$ , returns to the receiver level with representation

$$\Phi_2(\omega, p) = R_2(p)[1 - R_1^2(p)] \exp[2i\omega h_1/v_1(p)] \exp[2i\omega h_0/v_0(p)].$$

This procedure of splitting is repeated at each next interface. The chain of wave consisting of the sequence  $\Phi_1, \Phi_2, \dots, \Phi_N$  is by Bremmer (1951), called the principal wave, but in reflection seismology, it is called the primary reflection response. One reflection response is obtained for each slowness.

In the frequency-slowness domain, the  $N$  events of the dimensionless scattering amplitude can be modelled as

$$\Phi(\omega, p) = \sum_{n=1}^N \Phi_n(\omega, p) = \sum_{n=1}^N \hat{R}_n(p) \exp\left(2i\omega \sum_{m=0}^{n-1} \frac{h_m}{v_m(p)}\right), \quad (\text{A.2})$$

where each wave has the form of the product of an amplitude function and a delay function, both depending only on slowness. The frequency dependence comes only as a complex exponential due to the delay. The amplitude of the wave from the interface at depth  $z_n$  is

the product of the plane-wave reflection coefficient at  $z_n$  and the transmission coefficients encountered by the wave, namely

$$\hat{R}_1(p) = R_1(p), \quad \hat{R}_n(p) = R_n(p) \prod_{j=1}^{n-1} [1 - R_j^2(p)], \quad n = 2, 3, \dots, N. \quad (\text{A.3})$$

Performing an inverse Fourier transform over frequency, the dimensionless scattering amplitude in the time intercept-slowness domain becomes

$$\Phi(t, p) = \sum_{n=1}^N \hat{R}_n(p) \delta(t - \tau_n(p)), \quad (\text{A.4})$$

where  $\delta(t)$  is the Dirac delta function. The arrival time (called time intercept) of the primary reflection from depth  $z_n$  is

$$\tau_n(p) = 2 \sum_{m=0}^{n-1} \frac{h_m}{v_m(p)}.$$

(In the time-space domain,  $\tau$  is the time intercept of the tangent line with slope  $p$  with the time axis.)

## Appendix B. The Born potential

In the forward model developed in this paper, the Born approximation translates to setting the shift function in the forward model (31) to zero:

$$\xi = \xi_B(z) \equiv 0. \quad (\text{B.1})$$

Introduce the reference vertical slowness  $q = k_z/\omega = \sqrt{c_0^{-2} - p^2}$  and consider the Born approximation model

$$\Phi(\omega, p) = \int_0^\infty dz s(p, z) \exp(2i\omega q z), \quad (\text{B.2})$$

where the scattering function  $s$  is given in equation (20). By performing a partial integration over depth, one obtains

$$\Phi(\omega, p) = -\frac{i\omega q}{2} \int_0^\infty dz \alpha_B(p, z) \exp(2i\omega q z), \quad (\text{B.3})$$

where

$$\alpha_B(p, z) = -2 \ln[r_\rho(z)\Gamma(p, z)] \quad (\text{B.4})$$

is the single-scattering Born potential. Our objective is now to invert equation (B.3) for the Born potential.

Consider the inverse Fourier transform over the frequency of equation (B.3), that is,

$$\frac{2}{\pi} \int_{-\infty}^\infty d\omega \exp(-i\omega t) \frac{\Phi(\omega, p)}{-i\omega} = \int_0^\infty dz' \alpha_B(p, z') \frac{1}{2\pi} \int_{-\infty}^\infty d\omega' \exp\left[-i\omega' \left(\frac{t}{2q} - z'\right)\right], \quad (\text{B.5})$$

where  $\omega' = 2\omega q$ . By evaluating the integrals over frequency using equations (C.3) and (C.4), we obtain

$$4 \int_{-\infty}^{2z/v_0(p)} dt \Phi(t, p) = \int_0^\infty dz' \alpha_B(p, z') \delta(z - z'), \quad (\text{B.6})$$

where we have introduced  $z = t/(2q) = v_0 t/2$ , and  $v_0 = v_0(p) = c_0/\sqrt{1 - (c_0 p)^2}$  is the apparent velocity of the plane wave along the depth axis. The Born potential is thus related to

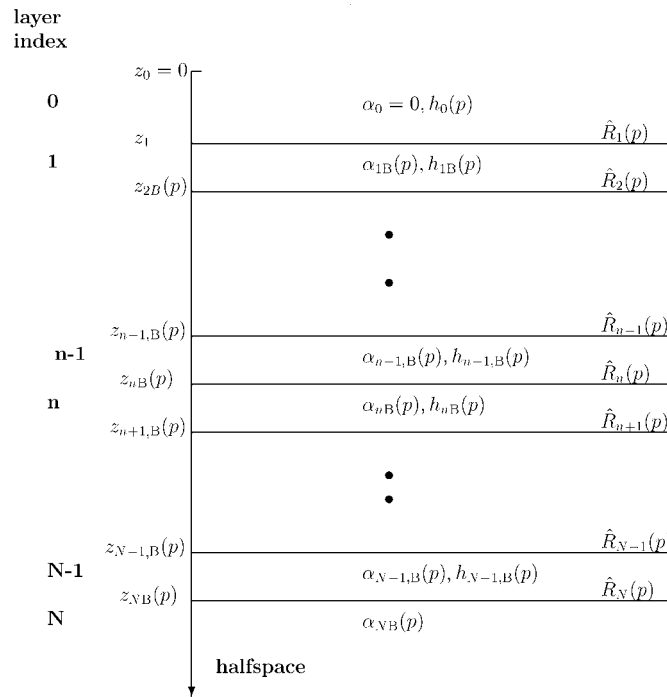


**Figure B1.** Layered medium that would be obtained from constant-velocity Born imaging.

the single scattering data as

$$\alpha_B(p, z) = 4 \int_{-\infty}^{2z/v_0(p)} dt \Phi(t, p). \quad (\text{B.7})$$

Equation (B.7) which is a key equation in the inversion procedure is known as constant-velocity migration or linear migration–inversion where primary reflection events are placed at depths computed linearly using their traveltimes together with the constant reference velocity. This is readily verified by substituting the primary reflection response (A.4) into equation (B.7). One obtains

$$\alpha_B(p, z) = 4 \sum_{n=1}^N \hat{R}_n(p) H(z - z_{nB}(p)), \quad (\text{B.8})$$

where  $H(z)$  is the Heaviside function, and  $z_{nB}$  is the depth at which the reference velocity  $c_0$  images the  $n$ th reflector:

$$z_{nB}(p) = v_0(p) \sum_{m=0}^{n-1} \frac{h_m}{v_m(p)}.$$

The Born-estimated thickness of layer  $m$  is thus

$$h_{mB}(p) = \frac{v_0(p)}{v_m(p)} h_m.$$

Observe that the first reflector is imaged at its correct depth for all slowness (or angle) traces,

$$z_{1B} = h_0 = z_1,$$

which is obvious since  $\alpha_c(z) = 0$  for  $z < z_1$ .

The depth model that would be obtained from the constant-velocity Born migration is shown in figure B1.

### Appendix C. Inverse Fourier transform of equation (32)

This appendix demonstrates that the inverse Fourier transform over the frequency of equation (32) yields equation (39). To this end, we make use of the Dirac delta function properties (Zwillinger 1996)

$$\int_{-\infty}^{\infty} dx f(x) \frac{d^n \delta(x-a)}{dx^n} = (-1)^n \frac{d^n f(a)}{dx^n}, \quad (\text{C.1})$$

$$\delta(ax) = \frac{1}{|a|} \delta(x), \quad (\text{C.2})$$

and the Fourier transform representation

$$\frac{d^n \delta(x-a)}{dx^n} = \frac{1}{2\pi} \int_{-\infty}^{\infty} dk (ik)^n \exp[ik(x-a)]. \quad (\text{C.3})$$

In addition, we make use of the Fourier integral transform

$$\frac{1}{2\pi} \int_{-\infty}^{\infty} dk \exp(-ikz) \frac{f(k)}{-ik} = \int_{-\infty}^z dt f(t). \quad (\text{C.4})$$

For any finite  $k$  and  $\xi(z)$ , express the exponential function  $\exp[ik\xi(z)]$  in equation (32) as an infinite series

$$\exp[-2ik\xi(z)] = \sum_{n=0}^{\infty} \frac{(-2ik)^n}{n!} \xi^n(z). \quad (\text{C.5})$$

Equation (32) is then written as

$$\frac{\Phi(\omega)}{-i\omega} = \frac{q}{2} \sum_{n=0}^{\infty} \frac{(-q)^n}{n!} \int_0^{\infty} dz' \alpha(z') (2i\omega)^n \exp(2i\omega q z'), \quad (\text{C.6})$$

where we have used that  $k_z = \omega q$ . Applying the inverse Fourier transform  $(2\pi)^{-1} \int d\omega \exp[-i\omega(2qz)]$  to equation (C.6), using equation (C.4), and interchanging the depth and frequency integrals give

$$4 \int_{-\infty}^{2qz} dt' \Phi(t') = q \sum_{n=0}^{\infty} \frac{(-q)^n}{n!} \int_0^{\infty} dz' \alpha(z') \frac{1}{2\pi} \int_{-\infty}^{\infty} d\omega (i\omega)^n \exp[i\omega q(z' - z)]. \quad (\text{C.7})$$

By using the Delta function properties (C.3), (C.2) and (C.1), and recalling that  $q = 1/v_0$ , one obtains equation (39).

### References

- Amundsen L, Reitan A and Arntsen B 2005a Geometric analysis of data-driven inversion/depth imaging *J. Seism. Explor.* **13** 51–62
- Amundsen L, Reitan A, Helgesen, H K and Arntsen B 2005b Data-driven inversion/depth imaging derived from approximations to one-dimensional inverse acoustic scattering *Inverse Problems* **21** 1823–50
- Berkhout A J 1982 *Seismic Migration, Imaging of Acoustic Wave Energy by Wavefield Extrapolation, A: Theoretical Aspects* 2nd edn (Amsterdam: Elsevier)
- Berkhout A J and Verschuur D J 2001 Seismic imaging beyond depth migration *Geophysics* **66** 1895–912
- Bejdoun W B and Mendes M 1989 Elastic ray-Born  $l_2$  migration/inversion *Geophys. J. Int.* **97** 151–60

- Bransden B H and Joachain C J 1989 *Introduction to Quantum Mechanics* (New York: Longman Scientific & Technical)
- Bremmer H 1951 The WKB approximation as a first term of a geometric-optical series *The Theory of Electromagnetic Waves: A Symposium* (New York: Interscience) pp 169–79
- Cao D 1989 Modélisation et inversion de données de sismique réflexion dans le domaine  $k$ - $\omega$  utilisant les approximations WKBJ et Born *Thèse de doctorat* L'Université de Paris
- Claerbout J F 1971 Toward a unified theory of reflector mapping *Geophysics* **36** 467–81
- Claerbout J F 1985 *Imaging the Earth's Interior* (Boston, MA: Blackwell Scientific)
- Clayton R W and Stolt R H 1981 A Born–WKBJ inversion method for acoustic reflection data *Geophysics* **46** 1559–67
- Cohen J K and Bleistein N 1977 An inverse method for determining small variations in propagation speed *SIAM J. Appl. Math.* **32** 784–99
- French W S 1975 Computer migration of oblique seismic reflection profiles *Geophysics* **40** 961–80
- Gazdag J 1978 Wave-equation migration by phase shift *Geophysics* **43** 1342–51
- Gelchinsky B, Berkovitch A and Keydar S 1999 Multifocusing homeomorphic imaging: Part 1. Basic concepts and formulae *J. Appl. Geophys.* **42** 229–42
- Glauber R J 1959 High-energy collision theory *Lectures in Theoretical Physics, Boulder 1958* ed W E Brittin and L G Dunham (New York: Interscience) pp 315–414
- Hubral P (ed) 1999 Macro-model independent seismic reflection imaging *J. Appl. Geophys.* **42** (3, 4) Special issue on the Karlsruhe Workshop
- Ikelle L T 1986 Inversion linéarisée de données de sismique réflexion dans l'espace de Fourier *Thèse de doctorat* L'Université de Paris
- Ikelle L T and Amundsen L 2005 *Introduction to Petroleum Seismology* (Tulsa, OK: Society of Exploration Geophysics)
- Innanen K A 2003 Methods for the treatment of acoustic and absorptive/dispersive wave field measurements *PhD Thesis* University of British Columbia
- Innanen K A and Weglein A B 2003 Simultaneous imaging and inversion with the inverse scattering series *Proc. 8th Int. Cong. of the SBGf and 5th Latin American Geophys. Conf.*
- Joachain C J 1975 *Quantum Collision Theory* (Amsterdam: North-Holland)
- Keys R G and Weglein A B 1983 Generalized linear inversion and the first Born theory for acoustic media *J. Math. Phys.* **24** 144–69
- Landa E, Gurevich B, Keydar S and Trachtman P 1999 Application of multifocusing method for subsurface imaging *J. Appl. Geophys.* **42** 283–300
- Lailly P 1984 The seismic inverse problem as a sequence of before stack migrations *Conf. on Inverse Scattering, Theory and Application* ed R Bednar and A Weglein (Philadelphia, PA: SIAM)
- Liu F, Weglein A B, Innanen K A and Nita B G 2005 Extension of the non-linear depth imaging capability of the inverse scattering series to multidimensional media: strategies and numerical results *Proc. 9th Int. Cong. of the SBGf and 6th Latin American Geophys. Conf.*
- Morse P M and Feshbach H 1953 *Methods of Theoretical Physics* (New York: McGraw-Hill)
- Ramirez A C and Weglein A B 2005 Progressing the analysis of the phase and amplitude prediction properties of the inverse scattering internal multiple attenuation algorithm *J. Seism. Explor.* **13** 283–301
- Santos L T dos, Ursin B and Tygel M 1996 Wave series expansion for a stratified fluid *Russ. Geol. Geophys.* **37** 23–45
- Schiff L I 1955 *Quantum Mechanics* (London: McGraw-Hill)
- Schneider W A 1978 Integral formulation for migration in two and three dimensions *Geophysics* **43** 49–76
- Secrest B G 1975 Migration techniques *Texas Instruments* TR 08-75-35
- Shaw S A 2005 An inverse scattering series algorithm for depth imaging of reflection data from a layered acoustic medium with an unknown velocity model *PhD Thesis* University of Houston
- Shaw S A, Weglein A B, Foster D J, Matson K H and Keys R G 2004 Isolation of a leading order depth imaging series and analysis of its convergence properties for a 1D acoustic medium *J. Seism. Explor.* **13** 99–120
- Shaw S A and Weglein A B 2004 A leading order imaging series for prestack data acquired over a laterally invariant acoustic medium: Analysis for bandlimited input data *Expanded Abstracts, 74th Ann. Int. Mtg., Soc. Expl. Geophys.* pp 2080–83
- Stolt R H 1978 Migration by Fourier transform *Geophysics* **43** 23–48
- Stolt R H and Weglein A B 1985 Migration and inversion of seismic data *Geophysics* **50** 2458–72
- Tarantola A 1987 *Inverse Problem Theory: Methods for Data Fitting and Model Parameter Estimation* (New York: Elsevier)
- Ursin B 1982 Quadratic wavefront and traveltimes approximations in inhomogeneous layered media with curved interfaces *Geophysics* **47** 1012–21
- Ursin B 1983 Review of elastic and electromagnetic wave propagation in layered media *Geophysics* **48** 1063–81

- Ursin B 1984 Seismic migration using the WKB approximation *Geophys. J. R. Astron. Soc.* **79** 339–52
- Ursin B 1987 The plane-wave reflection and transmission response of a vertically inhomogeneous acoustic medium *Deconvolution and Inversion* ed M Bernabini (Oxford: Blackwell) pp 189–207
- Ursin B *et al* 2004 Parameter inversion and angle migration in anisotropic elastic media *Geophysics* **69** 1125–42
- Weglein A B, Gasparotto F A, Carvalho P M and Stolt R H 1997 An inverse scattering series method for attenuating multiples in seismic data *Geophysics* **62** 1975–89
- Weglein A B, Foster D J, Matson K H, Shaw S A, Carvalho P M and Corrigan D 2002 Predicting the correct spatial location of reflectors without knowing or determining the precise medium and wave velocity: initial concept, and analytic and numerical example *J. Seism. Explor.* **10** 367–82
- Weglein A B, Araújo R V, Carvalho P M, Stolt R H, Matson K H, Coates R T, Corrigan D, Foster D J, Shaw S A and Zhang H 2003 Inverse scattering series and seismic exploration *Inverse Problems* **19** R27–83
- Weglein A B, Matson K H, Foster D J, Carvalho P M, Corrigan D and Shaw S A 2000 Imaging and inversion at depth without a velocity model: theory, concepts, and initial evaluation *Expanded Abstracts, 70th Ann. Int. Mtg., Soc. Expl. Geophys.*
- Zhang H and Weglein A B 2005 The inverse scattering series for tasks associated with primaries: depth imaging and direct non-linear inversion of 1D variable velocity and density acoustic media *Expanded Abstracts, 75th Ann. Int. Mtg., Soc. Expl. Geophys.* pp 1705–08
- Zwillinger D (ed) 1996 *Standard Mathematical Tables and Formulae* (New York: CRC Press)